Detection of miRNA cancer biomarkers using light activated Molecular Beacons

Gonçalves, Odete Sofia Lopes; Wheeler, Guy; Dalmay, Tamas; Dai, Houquan; Castro, Miguel; Castro, Patrick; García-Rupérez, Jaime; Ruiz-Tórtola, Ángela; Griol, Amadeu; Hurtado, Juan; Bellieres, Laurent; Bañuls, María José; González, Daniel; López-Guerrero, José Antonio; Neves-Petersen, Maria Teresa

Published in:
RSC Advances

DOI (link to publication from Publisher):
10.1039/c9ra00081j

Publication date:
2019

Document Version
Publisher's PDF, also known as Version of record

RSC Advances

PAPER

View Article Online
View Journal | View Issue

Cite this: *RSC Adv.*, 2019, **9**, 12766

Detection of miRNA cancer biomarkers using light activated Molecular Beacons†

Odete Sofia Lopes Gonçalves,[a] Guy Wheeler,[b] Tamas Dalmay,[b] Houquan Dai,[c] Miguel Castro,[c] Patrick Castro,[c] Jaime García-Rupérez,[d] Ángela Ruiz-Tórtola,[d] Amadeu Griol,[d] Juan Hurtado,[d] Laurent Bellieres,[d] María José Bañuls,[e] Daniel González,[e] José Antonio López-Guerrero[f] and Maria Teresa Neves-Petersen*[gh]

Early detection of cancer biomarkers can reduce cancer mortality rate. miRNAs are small non-coding RNAs whose expression changes upon the onset of various types of cancer. Biosensors that specifically detect such biomarkers can be engineered and integrated into point-of-care devices (POC) using label-free detection, high sensibility and compactness. In this paper, a new engineered Molecular Beacon (MB) construct used to detect miRNAs is presented. Such a construct is immobilized onto biosensor surfaces in a covalent and spatially oriented way using the photonic technology Light Assisted Molecular Immobilization (LAMI). The construct consists of a Cy3 labelled MB covalently attached to a light-switchable peptide. One MB construct contains a poly-A sequence in its loop region while the other contains a sequence complementary to the cancer biomarker miRNA-21. The constructs have been characterized by UV-Vis spectroscopy, mass spectrometry and HPLC. LAMI led to the successful immobilization of the engineered constructs onto thiol functionalized optically flat quartz slides and Silicon on Insulator (SOI) sensor surfaces. The immobilized Cy3 labelled MB construct has been imaged using confocal fluorescence microscopy (CFM). The bioavailability of the immobilized engineered MB biosensors was confirmed through specific hybridization with the Cy5 labelled complementary sequence and imaged by CFM and FRET. Hybridization kinetics have been monitored using steady state fluorescence spectroscopy. The label-free detection of miRNA-21 was also achieved by using integrated photonic sensing structures. The engineered light sensitive constructs can be immobilized onto thiol reactive surfaces and are currently being integrated in a POC device for the detection of cancer biomarkers.

Received 4th January 2019
Accepted 7th April 2019

DOI: 10.1039/c9ra00081j

rsc.li/rsc-advances

1 Introduction

The Globocan report pinpoints that in 2018 there were 18.1 million new cancer cases and 9.6 million cancer related deaths worldwide were registered despite advances in current therapies.[1,2] The number of new cases is expected to rise by 70% over the next two decades.[3] However, the WHO states that most cancer types have high cure rates when detected early and treated according to the best practices. Therefore, early and trustful detection tools for the implementation of preventive screening programs are crucial for reducing mortality rates.

Nanotechnology allows the engineering of biosensors with improved performances and functionalities. In particular, nanophotonic technology enables the creation of the core transduction elements of future high-performance biosensors providing high sensitivity, compactness and high integration level, shorter time to result, label-free detection, and reduced sample volumes. In today's point-of-care (POC) market, there is an ever-increasing demand for novel and more efficient devices for the early diagnosis of diseases, such as cancer.

New analysis devices for the detection of novel microRNA (miRNA) biomarkers are most useful and needed. miRNAs are a class of small non-coding RNAs (≈22 nucleotides) whose dysregulation has been correlated with a growing number of ≈400 human diseases,[4] including cancer, Alzheimer's, Parkinson's, diabetes, osteoporosis and cardiovascular diseases.

[a]*Medical Photonics Lab, Department of Health Science and Technology, Faculty of Medicine, Aalborg University, Fredrik Bajers Vej 7, DK-9220, Aalborg, Denmark*

[b]*School of Biological Sciences, University of East Anglia, Norwich Research Park, Norwich, NR4 7TJ, UK*

[c]*Biosynthesis, 612 East Main Street, Lewisville, TX 75057-4052, USA*

[d]*Nanophotonics Technology Center, Universitat Politècnica de València, Camino de Vera S/N, 46022 Valencia, Spain*

[e]*IDM, Instituto Interuniversitario de Investigación de Reconocimiento Molecular y Desarrollo Tecnológico, Departamento de Química, Universitat Politècnica de València, Camino de Vera S/N, 46022 Valencia, Spain*

[f]*Biología Molecular, Fundación Instituto Valenciano de Oncología, Valencia, Spain*

[g]*Department of Clinical Medicine, Aalborg University Hospital, Hobrovej 18-22, 9000 Aalborg, Denmark. E-mail: nevespetersen@gmail.com; Tel: +45 2252 2475*

[h]*Department of Biomedical Sciences and Medicine, Centre for Biomedical Research (CBMR), University of Algarve, Campus de Gambelas, 8005-139 Faro, Portugal*

† Electronic supplementary information (ESI) available. See DOI: 10.1039/c9ra00081j

Therefore, the use of miRNA biomarkers will allow the minimally invasive early diagnosis of almost 400 diseases. The technologies might be adapted to the diagnosis of any other disease associated with miRNA dysregulation by changing the probe immobilized on the sensor's surface.

Since the discovery of the loss of miRNA-15a and miRNA-16-1 in B-cell chronic lymphocytic leukaemia,[5] several studies reported changes of miRNA expression in several cancers.[6,7] Volinia *et al.* performed a large-scale miRNome analysis and identified a large portion of overexpressed miRNAs in solid tumours,[8] being miRNA-21, miRNA-191 and miRNA-17-5p significantly overexpressed in all the considered tumour types. However, they also validated particular miRNA signatures for each tumour. In recent years, miRNA expression profiling has been able to classify between healthy and tumour tissues and even between different tumour grades.[7,9–11] miRNAs have been found to be extraordinarily stable in plasma and serum samples.[12] Consequently, circulating miRNAs became potential candidates for blood-based biomarkers. Mitchell *et al.* showed that serum levels of miRNA-141 significantly discriminated patients with prostate cancer and healthy controls.[13] Moreover, other studies demonstrated the up-regulation of miRNA-21, miRNA-141, miRNA-200, miRNA-200c, miRNA-200b, miRNA-203, miRNA-205 and miRNA-214 in circulating cancer exosomes.[4] Some other miRNAs have also been found in extracellular fluids such as plasma serum, saliva and urine.[14]

The four varieties of cancer with higher incidence and mortality (≈2.7 million deaths worldwide) are: breast, prostate, lung and colorectal cancers.[15] miRNA-21 is overexpressed in most human tumours, including the above mentioned cancers. Our main goal is the detection of miRNA-21 using an engineered Molecular Beacon (MB) probe immobilized on a sensor surface using Light Assisted Molecular Immobilization (LAMI) technology.[16] Two MBs have been engineered: a model MB comprising a poly-A sequence in its loop region and a MB with a sequence complementary to miRNA-21 in its loop region. Crucial to the success of this work has been the conjugation of a light activated peptide (KAMHAWGCGGGC-NH_2) to the MB, with tryptophan in close spatial proximity to a disulphide bridge (Fig. 1). The peptide enables the immobilization of MB-peptide constructs with LAMI technology onto surfaces. LAMI is a photonic technology that allows for covalent and oriented immobilization of biomolecules onto thiol reactive surfaces, with μm and sub-μm spatial resolution.[17–23] This photonic technology presents some advantages over other immobilization techniques[24–28] as it does not require chemical or thermal steps to achieve covalent immobilization and it allows for spatially oriented immobilization. LAMI makes use of a conserved motif in proteins, *i.e.*, the close spatial proximity between aromatic residues (tryptophan, tyrosine and phenylalanine) and disulphide bridges.[16,29,30] UV excitation (275–295 nm) of aromatic residue's side chain induces electron ejection, which may react with the nearby disulphide bridge forming of a disulphide electron adduct.[31] Such short lived adduct will dissociate, leading to the formation of free thiol groups that will covalently bind peptides/proteins to thiol reactive surfaces. Any molecule can be immobilized with LAMI, even if they do not display aromatic residues or disulphide bridges, by tagging the molecule with a small peptide containing such motif.

The present paper shows that LAMI has successfully immobilized MB-peptide constructs onto sensor surfaces which have successfully hybridized with their respective complementary oligonucleotide. Non-complementary oligonucleotides have been used as controls. Hybridization kinetics have been monitored using steady state fluorescence spectroscopy. Detection of the immobilized MB construct's hybridization with the respective targets was visualised with confocal fluorescence microscopy (CFM) and using photonic bandgap (PBG) sensing structures. The use of these PBG structures allows for specific recognition of the target oligonucleotides through hybridization with the immobilized MB constructs on the surface of the PBG structures in a label-free and highly sensitive manner. The engineered light sensitive MB construct can be immobilized onto any thiol reactive surface and is being integrated in a photonic sensor device using the PBG structures for detection. The newly engineered MBs, their immobilization and bioavailability are hereby presented. We hereby demonstrate a proof-of-concept of the feasibility of the new integrated technology used to detect cancer biomarkers. Further studies are in progress in order to optimise the sensitivity of the newly engineered biosensor.

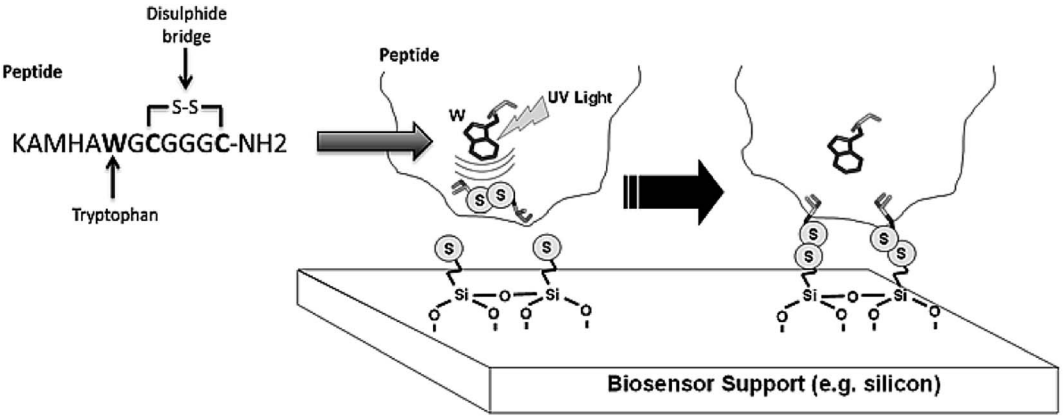

Fig. 1 Schematic representation of LAMI technology. The MB construct is coupled to a peptide which contains a tryptophan nearby a disulfide bridge. The disulfide bridge on the peptide is broken upon excitation of the nearby tryptophan allowing for covalent bonding of the MB construct onto the free thiol groups present on the biosensor support (*e.g.* SOI).

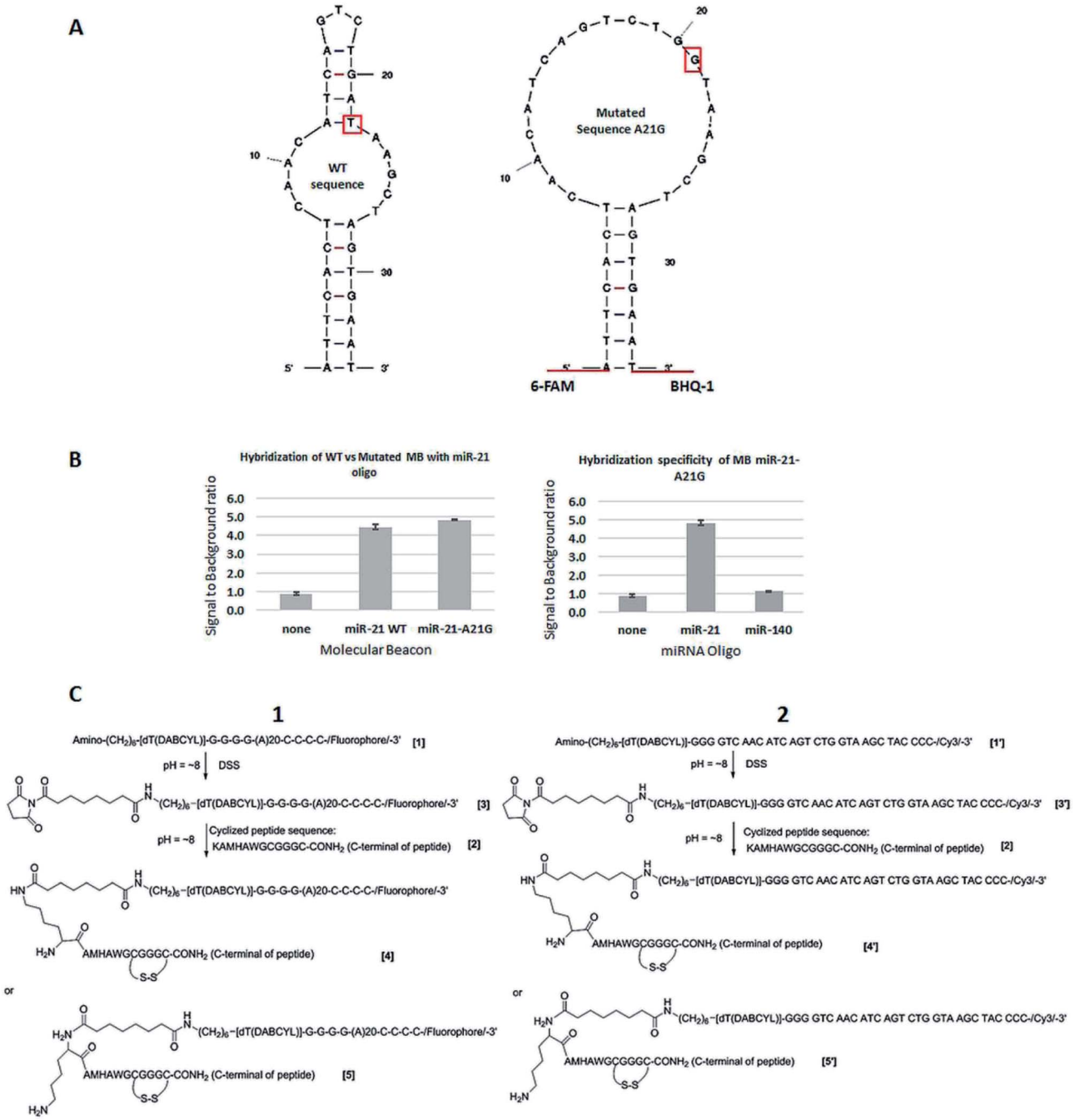

Fig. 2 Molecular Beacon sequence (A) and specificity (B) and chemical synthesis of the Molecular Beacon constructs (C). (A) Molecular Beacon design (UEA) with the wild type complementary sequence to miRNA-21 showed four base pairs predicted form within the loop (A). Changing the A at position 21 to a G (red box) removed the internal loop structure to form the desired stem-loop structure (B). (B) Fluorescence ratio of the MBs containing the wild type complementary sequence for miRNA-21 and with the single base change when detecting miRNA-21, compared with no miRNA target present (left). MiRNA-21 MB with the single base change could detect the miRNA-21 oligo but not a control oligo of miRNA-140 (right). (C) Engineered MB structures containing different oligonucleotide sequences. The MB is labeled with a fluorescent probe (Cy3) and contains a quencher (DABCYL) in close spatial proximity to the fluorophore when the MB loop is in its closed form. A peptide is coupled through a linker to the MB structure. This peptide has a disulphide bridge in close proximity to a tryptophan. This will allow for the LAMI immobilization of the MB constructs to the sensor surfaces. (A) MB structure containing G-G-G-G-(A)20-C-C-C-C in the loop region. (B) MB structure containing G-G-G-G-TCAA CATC AGTC TGGT AAGC TA-C-C-C-C in the loop region (oligonucleotide sequence complementary to miRNA21).

2 Materials and methods

2.1 Materials

The MBs and miRNA-21 oligonucleotide were purchased from Sigma-Aldrich, UK. KCl, $MgCl_2$ and Tris–HCl were also purchased from Sigma-Aldrich, UK. The MBs have a 5′ 6-FAM fluorophore and 3′ Black Hole Quencher-1 (BHQ-1),[32] which quenches 6-FAM fluorescence. The structure of the designed MBs is depicted in Fig. 2A.

The two engineered MB constructs (Cy3 labelled), their complementary and control sequences and the peptide KAMHAWGCGGGC-NH2 have been purchased from Biosynthesis (Texas, USA). The salts used to make PBS (sodium chloride, potassium chloride, sodium phosphate dibasic heptahydrate and potassium phosphate monobasic) were purchased from Sigma-Aldrich (Missouri, USA).

2.2 MB design and validation

MBs were designed with the mFold folding prediction software.[33] Fluorescence based assays using the MBs displayed in Fig. 2A were performed in white 96-well plates (Fisher, UK) in buffer consisting of 10 mM KCl, 5 mM $MgCl_2$ and 10 mM Tris–HCl pH 7.5.[34] Exposure to light was minimised to reduce fluorophore photobleaching and the samples were incubated at room temperature for 10 min before fluorescence readings were taken. Three wells for each condition were used and average readings were performed to calculate the fluorescence ratio (see, *e.g.*, Fig. 2B), which was calculated using the readings between wells containing the MB and the target miRNA oligo UACCACAGGGUAGAACCACGG and the MB alone.

2.3 Engineered MB construct structure

2.3.1 Selection of light activated peptide. The selected peptide was KAMHAWGCGGGC-NH2, being C cysteine (joined by a disulphide bridge), K lysine, A alanine, M methionine, H histidine, W tryptophan and G glycine. Its molecular mass is ≈1175 g mol^{-1}. UV excitation of the tryptophan leads to the disruption of the disulphide bridge, enabling the immobilization of the MB linked to this peptide onto the thiolized surfaces.

2.3.2 MB construct synthesis and characterization. The synthesis of the engineered MBs is depicted in Fig. 2C, schemes 1 and 2. The final construct is shown in Fig. 3 (left). In scheme 1 (Fig. 2C) is depicted the synthesis procedure for the poly-A MB and in scheme 2 (Fig. 2C) is depicted the procedure for the miRNA-21 specific MB. The peptide (step [2] and [2′] in schemes 1 and 2, respectively) was synthesized following standard solid phase peptide synthesis procedure to get the cyclized peptide and purified by RP-HPLC. Amino-C6-modified oligo (compound [1] in scheme 1 and compound [1′] in scheme 2) were

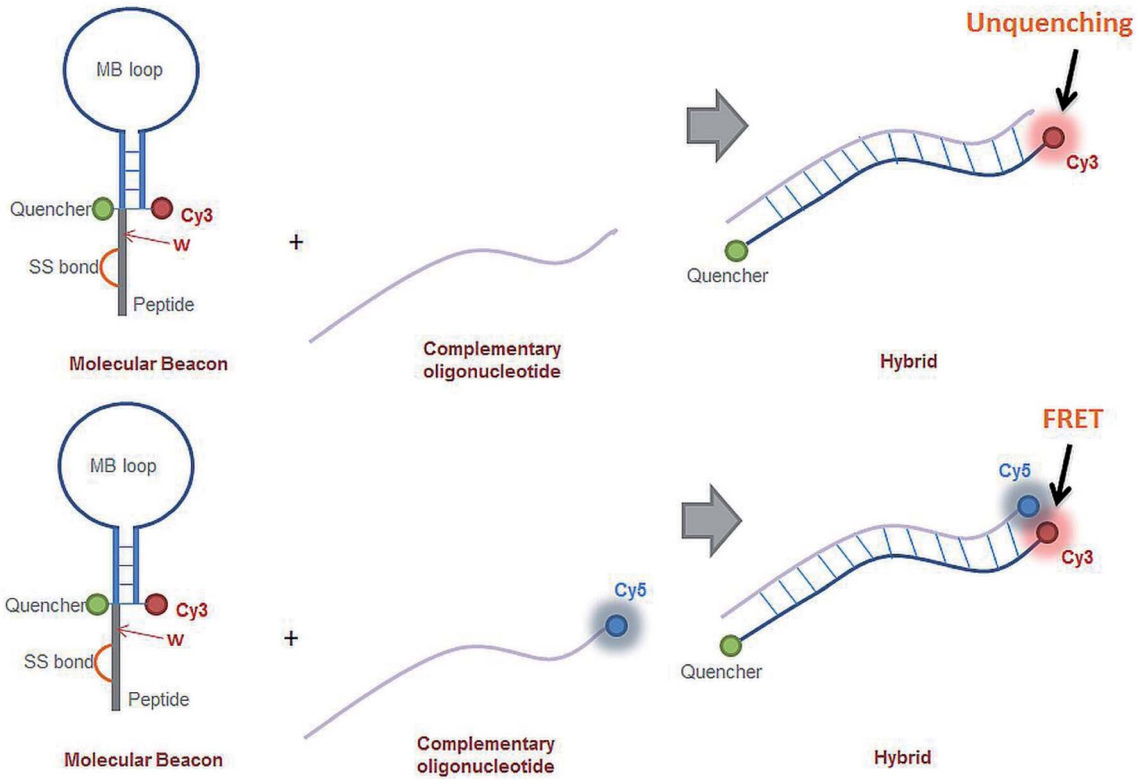

Fig. 3 Schematic representation of the detection strategies adopted for hybridization detection. Upon bonding with a complementary oligonucleotide sequence, the MB loop will open, allowing for the fluorophore to be distanced from the quencher present on the loop stem, leading to an increase of fluorescence intensity emission of Cy3 (top scheme). After the hybridization of the Cy5 labeled complementary oligonucleotide with the Cy3 labeled MB construct, the Cy3/Cy5 pair will be in close spatial proximity allowing for energy transfer from Cy3 (donor) to Cy5 (acceptor) (bottom scheme).

synthesized followed standard solid phase oligo synthesis procedure and purified by HPLC. The compounds [1] or [2] were dissolved into a mixture solution of DMSO–H_2O (1 : 2, v/v) and extra Disuccinimidyl Suberate (DSS) in DMSO was added. The mixture was incubated for several minutes at room temperature, precipitated by 30% of $NaClO_4$ in acetone, cooled down at −20 °C, and separated by centrifugation. After washing with acetone and drying, the precipitated products [3] or [3′] were dissolved into a mixture solution of DMSO–H_2O and extra peptide [2] in DMSO was added. The reaction mixture was incubated for 1–2 hours at 37 °C and precipitated by 30% of $NaClO_4$. After separation, the crude products [4], [5], or [4′] and [5′] were purified by RP-HPLC. The final product was characterized by Maldi-Tof Mass Spectrometry (MS) on Applied Biosystem (Model: Voyager DE-Pro; matrix solution: 10 mg mL^{-1} 3-hydroxypicolinic acid and 1 mg mL^{-1} diammonium hydrogen citrate in water) and the purity was assayed by RP-HPLC on Beckman (System Gold) and column (Phenomenex, Jupiter, C18, 300 Å, 10 μ, 150 × 3.0 mm). The assayed condition was wavelength: 260; flow rate: 0.8 mL min^{-1}; solvent A: 50 mM of triethylammonium acetate in water and solvent B : acetonitrile; with a gradient from 20% to 70% of solvent B in 20 minutes. The theoretical molecular weight (MW) was also calculated according to:

$$\text{Theoretical } M_w = M_{w(\text{oligonucleotide sequence})} + M_{w(\text{DSS linker residue})} + M_{w(\text{peptide})} \quad (1)$$

The calculated M_W was correlated to the M_W obtained through MS.

2.3.3 MB-peptide construct structures. The engineered MBs structure is depicted in Fig. 2C (steps [4], [5] in scheme 1 and [4′] [5′] in scheme 2, respectively) and illustrated in Fig. 3 (left). The poly-A MB loop region consists of 20 adenosine bases and 4 G–C base pairs form the stem of the MB (Fig. 2C, scheme 1, step [1]). The loop region of the miRNA-21 specific MB consists of TCAA CATC AGTC TGGT AAGC TA (Fig. 2C, scheme 2, step [1′]). This sequence is complementary to miRNA-21. Both MBs are coupled to a small peptide linked to one of the strands of the MBs' stem (Fig. 2C, scheme 1, steps [4] and [5] and scheme 2, steps [4′] and [5′]). Cy3 is attached to the 3′ end of the stem, being quenched by DABCYL, located on 5′ end of the stem. When the MB loop is closed (no hybridization), the presence of DABCYL in close spatial proximity to Cy3 will quench Cy3 emission. When hybridization occurs, the MB loop opens and Cy3 is separated from DABCYL, becoming unquenched, increasing the fluorescence intensity of Cy3 (Fig. 3, top scheme). The MB loop will only open when there is binding between the base pairs in the loop and the base pairs in the target sequence.

2.4 Preparation of MB constructs stock solutions

The poly-A MB and the miRNA-21 specific MB constructs were received in lyophilized form and resuspended in PBS 1× to a concentration of 10 μM. MB solutions were aliquoted and stored at −20 °C until use.

2.5 Preparation of oligonucleotide stock solutions for the engineered MB constructs

Three different oligonucleotide sequences were used in this study: two sequences are the complementary sequences to poly-A MB and to miRNA-21 specific MB. The third sequence is a non-complementary sequence to neither MBs (Table 1). The oligonucleotides were received in lyophilized form, and with and without a fluorescent label (Cy5), and resuspended in PBS 1× to a concentration of 10 μM. Oligonucleotide solutions were aliquoted and stored at −20 °C until use.

2.6 Steady-state fluorescence spectroscopy studies – hybridization kinetics

2.6.1 Presence of tryptophan in the peptide. The excitation (emission fixed at 350 nm) and emission (excitation at 295 nm) fluorescence spectra of a 0.1 μM poly-A MB-peptide sample in PBS 1× were monitored at room temperature, without stirring, in a 0.5 mL quartz cuvette. Measurements were performed in a Felix fluorescent RTC 2000 spectrometer (Photon Technology International, Canada, Inc. 347 Consortium Court London, Ontario N6E 2S8) with a T-configuration, using a 75 W Xenon arc lamp coupled to a monochromator.

2.6.2 Hybridization of the MB constructs with the complementary and control oligonucleotide using unquenching and Förster resonance energy transfer (FRET). Fluorescence based hybridization experiments performed with the poly-A MB constructs were carried out using the non-fluorescent oligonucleotide 5′-GTTTTTTTTTTTTTTTTTTTTC-3′. The detection strategy is depicted in Fig. 3 (top scheme) has been described in Section 2.3.3. 300 μL of the poly-A engineered MB samples were

Table 1 Oligonucleotide sequences used in this study

5′	Sequence (5′–3′)	Comments
Cy5 or unlabelled	GUAGCUUAUCAGACUGAUGUUGAC	RNA base, miRNA-21 sequence complementary to the miRNA21 specific MB sequence.
Cy5 or unlabelled	GAAAAAAAAAAAAAAAAAAAAAC	DNA base, sequence not complementary to the loop region of the model MB and of the miRNA-21 MB, this sequence is used as a hybridization negative control.
Cy5 or unlabelled	GTTTTTTTTTTTTTTTTTTTTC	DNA base, sequence complementary to the model MB sequence.
Cy5 or unlabelled	UACCACAGGGUAGAACCACGG	RNA base, miRNA-140 sequence non-complementary to the miRNA21 specific MB sequence (oligonucleotide used as a non-hybridization control on the section MB design and validation).

placed in a 0.5 μL quartz cuvette (0.1 mm optical pathway) at a final concentration of 0.1 μM and were illuminated at 548 nm, monitoring the fluorescence emission intensity at 562 nm for 2 min, at room temperature. The experiment was paused and a solution of the oligonucleotide (30 μL) was added to the poly-A MB solution (0.1 and 1 μM of complementary oligo were added to 0.1 μM of poly-A MB). Re-suspension was done with a pipette. Immediately after mixing, the solution was continuously illuminated at 548 nm and the increase fluorescence emission intensity at 562 nm (unquenching kinetics) was monitored for 1 h, at room temperature.

Hybridization between the miRNA-21 specific MB construct and the target sequence was monitored through FRET. Cy3 is present in the MB loop stem and the target oligonucleotides were Cy5 labelled. The emission spectra of Cy3 (donor) partially overlaps the excitation spectra of Cy5 (acceptor). When in close spatial proximity, this spectral overlap allows for energy transfer from the donor to the acceptor to occur. The spatial proximity requirement is fulfilled when hybridization takes place, allowing for the detection of the specific binding between the MB and the target oligonucleotide (Fig. 3, bottom scheme). Hybridization experiments with the miRNA-21 specific MB were carried out using the Cy5 labelled synthesized oligonucleotide, 5′-CAG UUG UAG UCA GAC UAU UCG AUG-3′, complementary the MB's loop sequence. 300 μL of the miRNA-21 specific MB samples were prepared in a 0.5 μL quartz cuvette (0.1 mm optical pathway) at a concentration of 0.1 μM in PBS 1× and illuminated at 488 nm, monitoring the fluorescence emission intensity at 670 nm for 2 min, at room temperature. Cy5 absorption is non-existent at 488 nm, whereas for Cy3 is in the order of 17% of its maximum absorbance.[35] Cy5 fluoresces maximally at 670 nm, the wavelength monitored during these experiments. Thus, the recorded fluorescence emission intensity results from energy transfer between Cy3 (donor) and Cy5 (acceptor).

The experiment was paused and 30 μL of a solution of Cy5 labelled oligonucleotide solution was added to the miRNA-21 specific MB solution (0.1 and 1 μM, respectively). Re-suspension was done with a pipette. Immediately after mixing, the solution was again continuously illuminated at 488 nm and the fluorescence emission intensity at 670 nm was monitored for 1 h, at room temperature. As a non-hybridization control, a 30 μL of a solution of Cy5 labelled non-complementary oligonucleotide poly-A was added and the fluorescence change was monitored.

2.7 Sensor surfaces

Two kinds of sensor surfaces were used to immobilize the light sensitive MB constructs: optically flat quartz slides and Silicon on Insulator (SOI) chips (with and without photonic bandgap (PBG) sensing structures). Optically flat quartz slides were purchased from ArrayIt (SuperClean 2, SCM2) and SOI chips (with and without PBG sensing structures) were provided by the Universitat Politècnica de València. The PBG structures present in some of the SOI chips used in this study are generated by introducing a periodic modulation in the refractive index of the photonic structure. In this type of PBG sensing structure, its periodicity gives rise to the presence of a spectral range where the propagation of the light is forbidden, the so-called photonic bandgap (PBG). When the refractive index of the surroundings of the PBG sensing structure will change due to the presence of the target analytes (the miRNA target in our case), the PBG spectral position will shift depending on the target analyte concentration.

The photonic chips used in the experiments comprised several PBG sensing structures of dimensions width w = 460 nm, height h = 220 nm, period a = 380 nm and length of the transversal elements w_e = 1500 nm. The PBG sensing structures where organized in pairs, where two different widths of the transversal elements were used for each structure (w_i = 120 nm and w_i = 140 nm). Each chip contained 4 PBG sensor pairs. The photonic chips were fabricated using e-beam lithography and inductively coupled plasma etching to transfer the designs to the top silicon layer. An image of one of the fabricated PBG sensing structures is shown in Fig. 4. Shallow etch 1D grating couplers where fabricated at the accesses of the photonic structures in order to vertically couple the light to/from the chip inputs/outputs. Finally, a top 400 nm-thick SiO_2 upper cladding is deposited over the photonic chip in order to increase the robustness of the photonic structures and to avoid their damage when the microfluidic cell required to flow the reagents over the chip is placed; a channel is opened in the SiO_2 upper cladding in the positions where the PBG sensing structures are placed in order be in contact with the samples to be analysed.

2.7.1 Thiolation of sensor surfaces. The surfaces were chemically modified by silanization according to a method described elsewhere,[16] except that the surfaces were not treated with chromosulfuric acid prior to silanization.

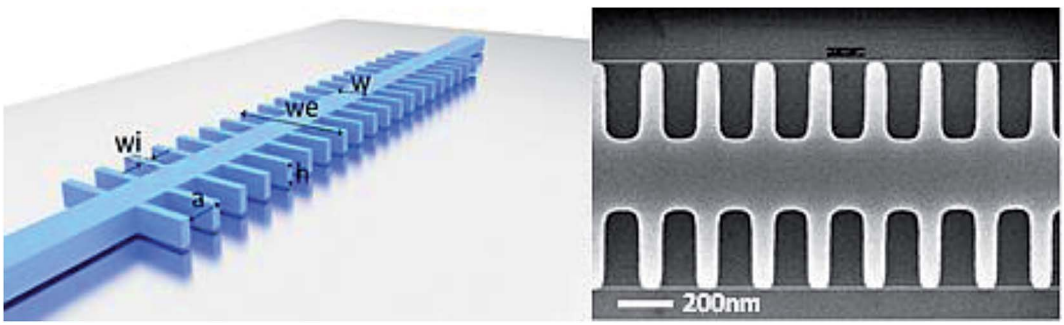

Fig. 4 Photonic bandgap (PBG) sensing structures. (Left) Schematic representation of the PBG sensing structure used to carry out the photonic miRNA sensing experiments. (Right) Scanning Electron Microscope (SEM) image of one of the PBG sensing structures fabricated in this work.

2.8 Illumination setup

A scheme of the experimental system[36] is shown in Fig. 5A. The femtosecond (fs) laser Tsunami XP (Spectra-Physics), is pumped by the Millennia eV (Spectra-Physics). Typical operation is around 840 nm with maximum average power of 4 W. The Tsunami output (~100 fs pulses at 80 MHz) is frequency tripled in a harmonic generation module (Spectra-Physics) to produce ~280 nm UV fs pulses with an efficiency of ~10%. The fundamental at 840 nm and the third harmonic at 280 nm are routed *via* separate paths into the experimental system. Each beam passes through a computer controlled variable attenuator consisting of a half-wave plate, mounted in a motorized rotation stage (PR50CC, Newport) and followed by a polarizing beam cube. After each attenuator, a fused silica beam sampler is used to direct a portion of the beam onto a photodiode (PD-300R-3W and PD-300R-UV, OPHIR) for power monitoring. The beam then passes through safety shutters (LS6S2ZM1, VINCENT ASSOCIATES) to control exposure to the sample. Only the 280 nm beam has been used in the present study.

2.8.1 Photonic immobilization of MB constructs using LAMI technology. A droplet of each engineered MB (1 μL) was placed on the surface of the optically flat thiol derivatized surfaces. After drying at room temperature, the sample was placed in the sample holder of the illumination setup (Fig. 5B). Samples were illuminated at 280 nm according to an array pattern (500 × 500 μm) on the thiol derivatized quartz slides and according to a line pattern (50 lines with 50 μm separation) on the thiol derivatized SOI surfaces (without PBG sensing structures). The patterns were uploaded to the controlling stage software in a bitmap image format. Illumination was performed at 100 μm s^{-1} with a focused laser beam (focused light) through a 40× UV objective. The illumination power used was 20 or 40 μW. For biofunctionalization of the SOI chips with PBG sensing structures, a droplet of mi-RNA-21 MB construct was place two

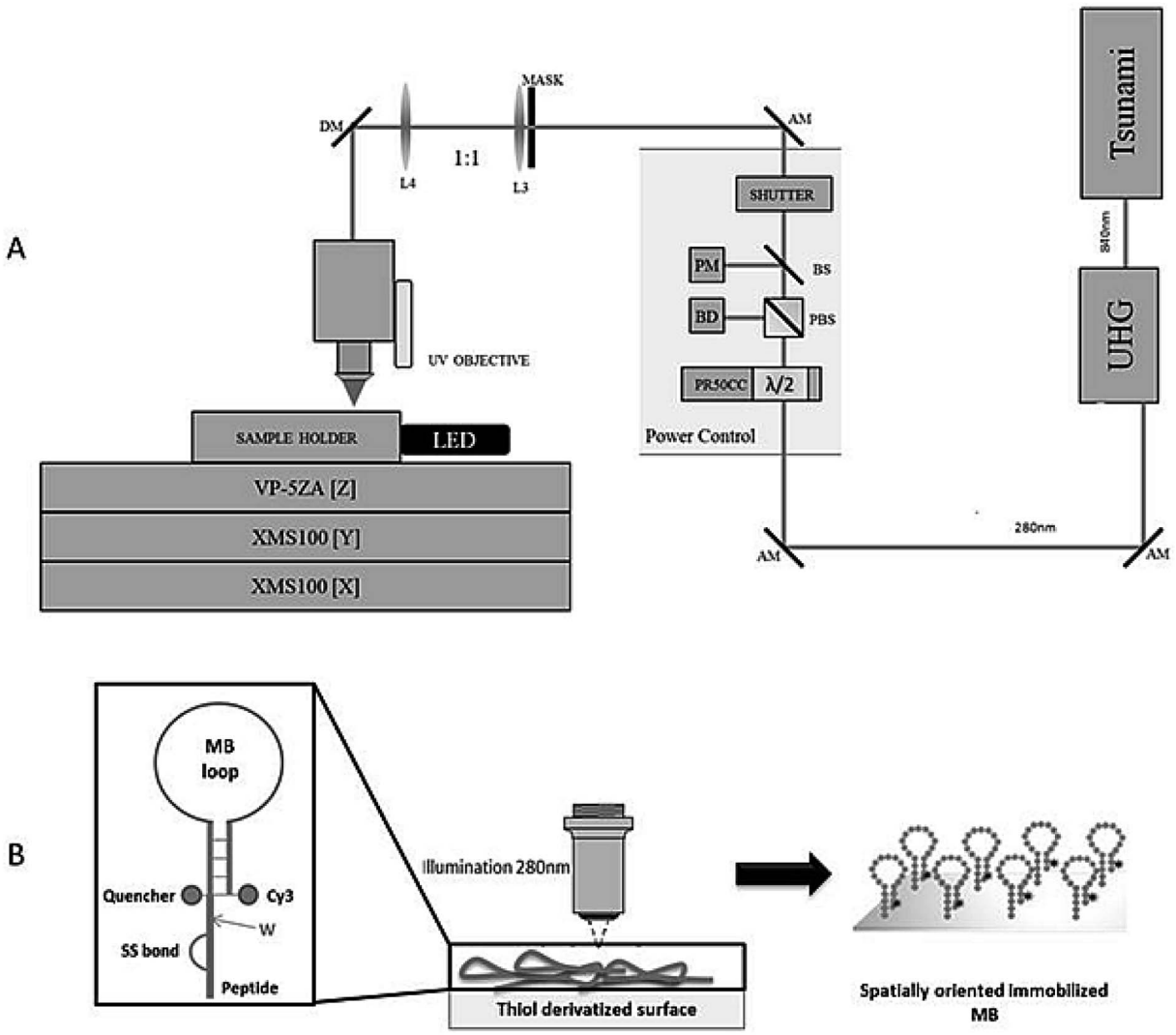

Fig. 5 Schematic representations of the illumination setup and methodology. (A) Schematic description of the laser beam pathway through the UHG module and into the UV objective where the 280 nm light is focused on the sample placed onto the moving sample holder. (B) Illustration of the LAMI procedure carried out using the illumination setup and applied to the engineered MB. LAMI leads to covalent and oriented immobilization of the MB constructs which will be ready to detect the specific miRNA targets.

pairs of these structures and illuminated continuously for 1 h at 280 nm (diffuse light). The remaining pairs of PBG structures did not contain miRNA-21 specific MB construct and were used as controls. After illumination, the immobilized samples were washed overnight with PBS 1× plus 0.1% Tween 20 detergent, rinsed with PBS 1× and dried with compressed air.

2.9 Confocal fluorescence microscopy (CFM) studies – fluorescent label detection

2.9.1 Imaging the immobilized MB constructs onto optically flat quartz slides and SOI surfaces without PBG sensing structures. An inverted confocal fluorescence microscope (LEICA TCS SP5) was used to visualize the patterns. To visualize the immobilized patterns, the immobilized poly-A MB was excited using the 543 nm laser line form the HeNe laser and Cy3 emission was visualized from ≈570 to 650 nm. Even though the fluorophore is quenched by DABCYL when the MBs are immobilised and non-hybridized with the respective complementary oligonucleotides, their residual fluorescence is still detected.

2.9.1 Pattern imaging of immobilized and hybridized MB construct onto optically flat quartz slides and SOI surfaces without PBG sensing structures. Hybridization of the immobilized patterns of both poly-A MB and of miRNA-21 specific MB constructs with their respective complementary oligonucleotide was detected by FRET. The immobilised MB constructs patterns (labelled with Cy3) were incubated with 10 μM of their respective oligonucleotide (labelled with Cy5) for 1 h at 37 °C. After incubation, the arrays were rinsed with PBS 1× and gently dried with compressed air. The same procedure was also applied using a non-complementary oligonucleotide (poly-A sequence). The arrays were then excited using the 543 nm laser line from the HeNe laser and emission was imaged by CFM by two separate PMT's registering emissions from ≈570 nm to 650 nm (Cy3 emission) and from ≈700 nm to 780 nm (Cy5 emission), respectively. An overlap of these two emission channels was carried out to detect co-localization of Cy3 labelled MB and of Cy5 labelled complementary oligo. Patterns were visualized through an UV 20× objective.

2.9.3 Photonic-based detection on SOI surfaces with PBG sensing structures biofunctionalised with miRNA-21 specific MB construct – label-free detection. The biofunctionalized SOI chip with PBG sensing structures is assembled with a polydimethylsiloxane (PDMS) flow cell having a flow channel (400 μm-wide and 50 μm-high). This assembled chip is then placed in an automated optical characterization setup where the spectral response of all the photonic sensing structures in the chip is continuously registered. A fiber aspheric collimator (Thorlabs CFS2-1550-APC) is used to couple the light from a continuous sweep tunable laser (Keysight 81980A) to the access grating couplers. An infrared (IR) camera (Xenics Xeva-1.7-320) is used to measure the light from the output grating couplers, which is collected with an objective (20× Olympus Plan Achromat, 0.4 NA). The continuous sweep of the laser and the image acquisition of the IR camera *via* a trigger signal are synchronized by a software programed in LabVIEW which is able to control the interrogation platform. This synchronization allows for the acquisition of the spectra of the photonic structures with the desired spectral resolution.

The configuration for spectra acquisition was set to a range between 1520 nm and 1620 nm with a sweeping speed of 10 nm s^{-1} and a spectral resolution of 20 pm. Using a constant flow rate of 20 μl min^{-1}, the target oligonucleotide solutions are flowed using a syringe pump working in withdraw mode.

2.10 Data analysis

All data analysis, plotting and fitting procedures were done using Origin 8.1 (OriginLab Corporation, Northampton, MA, USA) and MATLAB (MathWorks, Inc. Natick, MA, USA). Fluorescence emission intensity profiles and the 3D surface plot of the immobilized and hybridized MB patterns, imaged by CFM, were obtained using ImageJ 1.50i.

2.10.1 Emission spectra and excitation spectra. Emission and excitation spectra were smoothed using a 10 points adjacent averaging. All fluorescence spectra obtained were Raman corrected by subtracting the buffer spectra. Normalized emission and excitation spectra were obtained by dividing each data point by the maximum intensity value in each spectrum.

2.10.2 Hybridization kinetic traces. The hybridization curves obtained for both poly-A MB and miRNA-21 specific MB were normalized to their maximum fluorescence emission intensity.

2.11 Fitting procedures

2.11.1 Hybridization kinetic traces – emission recorded as a function of time at 562 nm and 670 nm upon 548 nm continuous excitation. Each hybridization curve was acquired upon addition of the complementary oligonucleotide and monitored upon continuous illumination at 548 nm and 488 nm for 1 h (Fig. 6A and B, respectively). The fluorescence emission intensity data obtained upon addition (at 120 s) of the complementary oligonucleotide were fitted using a double exponential growth model given by the function $F(t) = y_0 + A_1(1 - \exp(-x/t_1)) + A_2(1 - \exp(-x/t_2))$, where y_0 is the offset value, A_1 and A_2 are the amplitudes and t_1 and t_2 are the rate constants of each phase. The errors associated to each parameters and the root mean square error determined the goodness of the fit. The fractional intensity (f_i) of each time constant is given by $f_i = A_i t_i / \Sigma_i A_i t_i$, where A_i is the amplitude (pre-exponential factor) and t_i is the time constant. The mean time constant was calculated according to $\langle t \rangle = \Sigma_i f_i t_i$. These parameters are presented in Table 2. The hybridization curve obtained for 0.1 μM poly-A MB + 1 μM complementary oligonucleotide (poly-T) did not fit well to either a single or double exponential growth model (due to a fast rise of the curve that led to few points before the plateau region) thus, no fitting is presented. The kinetics for hybridization of the MB constructs with the respective complementary oligonucleotide were assumed to follow a two-state mechanism where [MB] + [complementary oligonucleotide] ↔ [MB · complementary oligonucleotide].

2.12 Image treatment

An area of the CFM images was selected and analysed to obtain the accumulated average fluorescence emission intensity

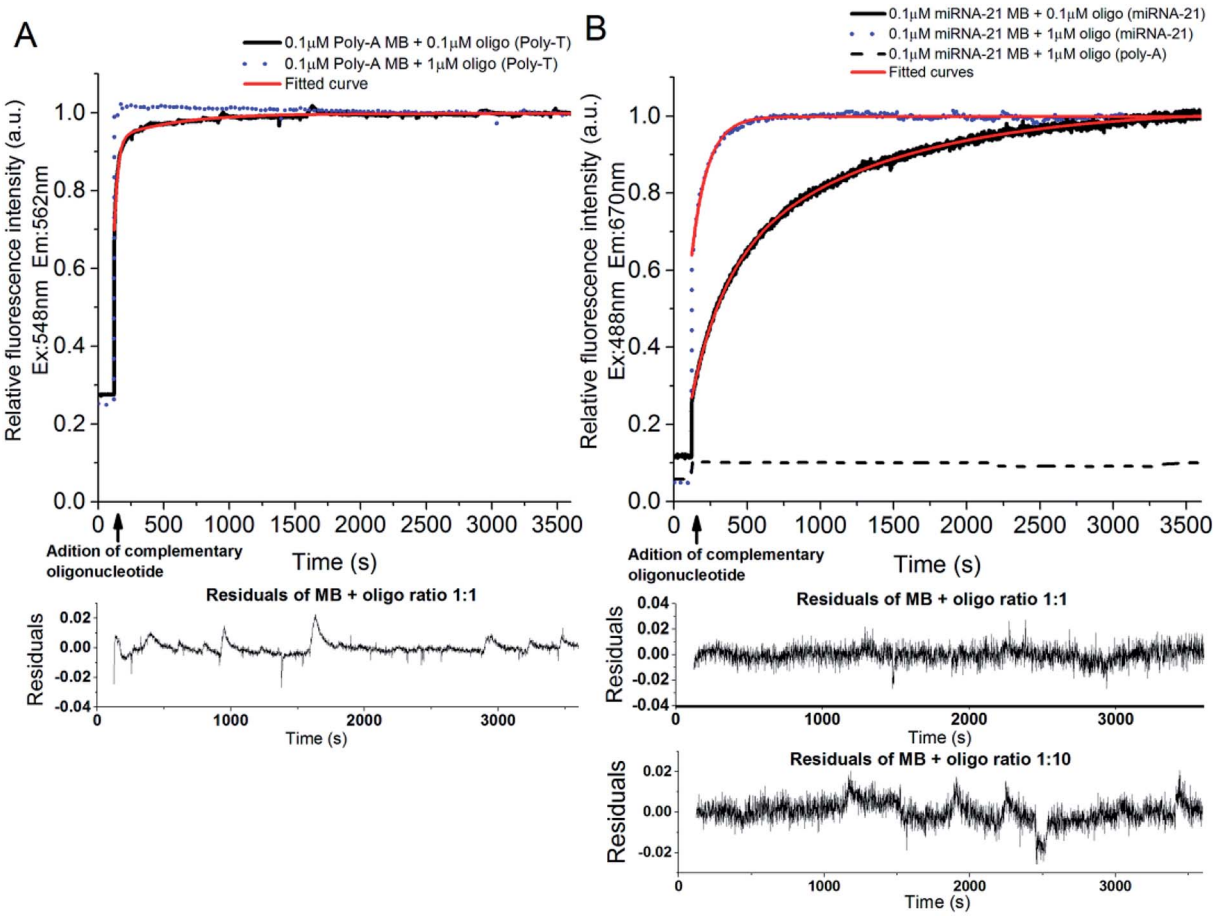

Fig. 6 Monitoring the binding kinetics between each MB and its respective complementary oligonucleotide sequence through unquenching (A) and FRET (B). The following concentration ratios were used: 0.1 μM MB + 0.1 μM complementary oligo (ratio 1 : 1) and 0.1 μM MB + 1 μM complementary oligo (ratios 1 : 10). The hybridization curves were fitted according to a double exponential growth model $F(t) = y_0 + A_1(1 - \exp(-x/t_1)) + A2(1 - \exp(-x/t_2))$. The fitted curves are represented in red and the residuals are represented bellow each curve. (A) Binding kinetics between Cy3 labelled poly-A MB construct and its complementary oligonucleotide sequence (poly-T) monitored by C3 fluorescence emission intensity signal. (B) Binding kinetics between Cy3 labeled miRNA-21 MB construct and the Cy5 labeled complementary oligonucleotide (miRNA-21) monitored by C5 fluorescence emission intensity signal. Binding kinetics between Cy3 labeled miRNA-21 MB and Cy5 labelled non-complementary poly-A was monitored as a non-hybridization control.

profiles. These profiles result in a 2D display of pixel intensity along a selected area of the image. For the 3D surface plot, a plot derived from the pixel intensity displayed in the selected area of the image was created and adjusted for lighting, perspective and smoothing.

3 Results

3.1 MB selection and validation

MB design showed unwanted base pairing within the loop (Fig. 2A, left). A single base change was required to open the structure out into the desired loop to allow access by the target miRNA-21. As seen in Fig. 2A (right), a mutation of A at position 21 to a G removed this unwanted base pairing, whilst still retaining the hybridization potential with the T in the miRNA-21 sequence from G:T pairing. Specificity of the MB for miRNA-21 was tested by comparing the results using a MB containing the wild type loop sequence complementary to miRNA-21 against that with the A–G base change necessary to remove the unwanted base pairing, and a negative control using an RNA oligo of the unrelated miRNA-140. The concentrations used were 25 nM of miRNA-21 specific MB and 50 nM of target miRNA (see paragraph ahead, justifying this choice of concentrations). As seen in Fig. 2B (left), opening of the loop with the single base change makes the MB more able to hybridize with the target miRNA, with an increase in fluorescence ratio of ≈8.6%, compared with the MB containing the wild type sequence. No increase in fluorescence ratio was observed when hybridizing the miRNA-21 specific MB with miRNA-140 (Fig. 2B, right).

Optimization experiments were performed to find the concentration of the MB necessary for fluorescence detection of target miRNA. The fluorescence emission intensity of different concentrations of miRNA-21 specific MB (labelled with 6FAM but without quencher) was monitored and the fluorescence ratio calculated as the fluorescence reading of the MB against

Table 2 Parameters obtained according to the double exponential fitting model $F(t) = y_0 + A_1(1 - \exp(-x/t_1)) + A2(1 - \exp(-x/t_2))$[a]

Y offset	Rate constant (s^{-1})	Fractional intensity (%)	Amplitude
Poly-A MB (unquenching)			
Poly-A MB + poly-T oligo (1 : 1)			
$y_0 = -19.323 \pm 1.116$	t_1 (slow phase) = 465.272 ± 6.453	$f_1 = 6$	$A_1 = 0.081 \pm 0.001$
	t_2 (fast phase) = 27.757 ± 0.326	$f_2 = 94$	$A_2 = 20.240 \pm 1.115$
	$\langle t \rangle = 55.262$		
miRNA-21 MB (FRET)			
miRNA-21 MB + miRNA-21 oligo (1 : 1)			
$y_0 = -0.021 \pm 0.004$	t_1 (slow phase) = 1120.800 ± 9.225	$f_1 = 83$	$A_1 = 0.499 \pm 0.003$
	t_2 (fast phase) = 210.142 ± 2.496	$f_2 = 17$	$A_2 = 0.543 \pm 0.003$
	$\langle t \rangle = 966.487$		
miRNA-21 MB + miRNA-21 oligo (1 : 10)			
$y_0 = -13.896 \pm 4.721$	t_1 (slow phase) = 126.854 ± 1.374	$f_1 = 22$	$A_1 = 0.784 \pm 0.019$
	t_2 (fast phase) = 24.449 ± 1.750	$f_2 = 78$	$A_2 = 14.111 \pm 4.706$
	$\langle t \rangle = 47.366$		

[a] *Y* offset (y_0), amplitude (A_i), rate constants (t_i), intensity fraction (f_i) and average rate constant ($\langle t \rangle$) for hybridization of poly-A and miRNA-21 specific MB constructs with the respective complementary oligonucleotides (ratios 1 : 1 and 1 : 10).

that of the assay buffer (Fig. S1A†). For further optimizations, 25 nM of 6-FAM labelled miRNA-21 specific MB was used since the fluorophore emission intensity was clearly detectable. To optimize the concentration of miRNA oligo in the assay, 25 nM of MB and a range of miRNA concentrations from 25–1000 nM were used. As shown in Fig. S1B† miRNA oligo at 50 nM and above produced fluorescence ratios clearly detectable above those of the MB or assay buffer alone. For further experiments, 25 nM MB and 50 nM miRNA oligo were used (Fig. 1, scheme 3).

3.2 Engineered MB constructs: synthesis and characterization

The purity level of the MB coupled to the peptide obtained by HPLC was >96% for the poly-A MB construct and >97% for the miRNA-21 MB construct (Fig. S2†). The M_W of the MB constructs was determined by MS (Fig. S3†). Data obtained for the poly-A MB construct (Fig. S3,† upper panel) shows a clearly defined peak corresponding to a M_W of 11 384.78 Da, matches the theoretical M_W (11 384.84 Da). The same was observed for the MS data obtained for the miRNA-21 construct (Fig. S3,† lower panel), where a sharp peak shows a M_W of 12 001.09 Da, which matches the calculated M_W (12 000.16 Da).

3.3 Steady state fluorescence studies – hybridization kinetics

3.3.1 Presence of tryptophan in the peptide construct. In Fig. S4† are depicted the fluorescence excitation and emission spectra of the poly-A MB upon excitation at 295 nm and fixed emission at 350 nm. The fluorescence emission spectrum presents maximum intensity peak at 353 nm, whereas the maximum fluorescence intensity peak of the excitation spectra is at 298 nm. These spectral features are characteristic of tryptophan, proving its presence in the tag construct.

3.3.2 Hybridization studies using poly-A and miRNA-21 specific MB constructs. In Fig. 3 is depicted the strategy used for the detection of the target miRNA by the MB constructs (as explained in Section 2.6.2). The binding kinetics between the poly-A MB and the respective complementary non-labelled oligonucleotide were studied at different concentrations: 0.1 and 1 μM of complementary oligonucleotide poly-T were added to 0.1 μM of poly-A MB (ratios 1 : 1 and 1 : 10, respectively). The binding kinetics were monitored following the increase of fluorescence emission intensity as a function of time after adding the complementary oligonucleotide to the poly-A MB solution. The MB loop opens upon binding with the complementary oligonucleotide resulting in an increase of Cy3 emission due to separation between the fluorophore (Cy3) and the quencher (dtDABCYL), (Fig. 3A). In Fig. 6A are displayed the kinetic curves obtained upon monitoring the fluorescence emission intensity of Cy3 ($\lambda_{excitation}$ = 548 nm, $\lambda_{emission}$ = 562 nm) and the respective fitted curve for the hybridization at a ratio of 1 : 1. The fitting parameters are described in Table 2. The residual values for this fitting are randomly distributed around 0 (Fig. 6A, lower panel).

The hybridization curve obtained for ratio 1 : 1 demonstrates a fast phase with a rate constant of 27.757 ± 0.326 s^{-1} and an amplitude of 20.240 ± 1.115 followed by a slow phase with a rate constant of 465.272 ± 6.453 s^{-1} and an amplitude of 0.081 ± 0.001. The calculated fractional intensity for the fast rate constant was 94% and for the slow rate constant was 6%. Thus, the average rate constant obtained for this ratio was 55.3 s^{-1}, indicating a reaction where the [MB · complementary oligonucleotide] equilibrium is reached fast. Increasing the ratio to 1 : 10, the reaction rate is much faster (Fig. 6A, blue dotted lines). A good fitting was not achieved for the hybridization curve obtained at the ratio 1 : 10, however the curve shape shows a fast increase of fluorescence intensity reaching a plateau within ≈150 s.

The binding kinetics between the miRNA-21 specific MB and its respective complementary oligonucleotide were monitored through FRET between Cy3 (stem of the MB loop) and Cy5 (complementary oligonucleotide) (Fig. 3B). In Fig. 6B is

depicted the binding curve between the miRNA-21 specific MB and the oligonucleotide at different concentrations: 0.1 and 1 μM of oligonucleotide miRNA-21 were added to 0.1 μM of miRNA-21 specific MB (ratios 1 : 1 and 1 : 10, respectively). The increase of fluorescence emission intensity of Cy5 is monitored as a function of time ($\lambda_{excitation} = 488$ nm, $\lambda_{emission} = 670$ nm) before and after adding the oligonucleotide. The respective fitted curves are also depicted in Fig. 6B and the derived fitting parameters can be found in Table 2. The residual values for these fitting are randomly distributed around 0 (Fig. 6B, lower panels).

The curve obtained for the hybridization of the miRNA-21 specific MB with the complementary oligonucleotide at a ratio of 1 : 1 shows an initial fast phase with a rate constant of $210.142 \pm 2.496\ s^{-1}$ and an amplitude of 0.543 ± 0.003 followed by a slower phase with a rate constant of $1120.800 \pm 9.225\ s^{-1}$ and an amplitude of 0.499 ± 0.003. However, at a ratio of 1 : 10, the obtained fast rate constant was $24.449 \pm 1.75\ s^{-1}$ with an amplitude of 14.111 ± 4.71 and the slower rate constant was $126.854 \pm 1.37\ s^{-1}$ with an amplitude of 0.784 ± 0.02. At ratio (1 : 1), the calculated fractional intensity is higher for the slow rate constant (83%) whereas at a ratio of 1 : 10, the higher calculated fractional intensity was obtained for the fast rate constant (78%). Thus, the obtained average rate constants for ratios 1 : 1 and 1 : 10 were $966.5\ s^{-1}$ and $47.4\ s^{-1}$, respectively. This indicates that at the lower molar ratio of 1 : 1, the [MB · complementary oligonucleotide] equilibrium (plateau region) is reached at a slower pace, as expected. However, the difference registered between ratios for the miRNA-21 specific MB (Fig. 6B) hybridization is much higher then what is observed for the poly-A MB (Fig. 6A). The fluorescence emission intensity of miRNA-21 specific MB upon addition of a non-complementary poly-A oligonucleotide was also monitored (Fig. 6B, black dashed line). No hybridization occurs, as expected.

3.4 Photonic immobilization using LAMI and visual detection using CFM – fluorescent label detection

3.4.1 Photonic immobilization of poly-A MB construct onto optically flat thiol derivatized quartz surfaces. The poly-A MB construct was illuminated with 280 nm light according to an array pattern using the laser system setup described in Section 2.8. After overnight washing, the array was visualized by CFM and is depicted in Fig. 7A. It is possible to observe that the poly-A MB construct was successfully immobilized according to an array pattern (500 × 500 μM). A 3D projection of the immobilized array is shown in Fig. 7B. In this analysis, the area containing the immobilized array was selected (yellow lines). The software creates an interactive surface plot, where the height of the plot is interpreted from the pixel intensity of the selected area. Spatially well-defined and homogeneous fluorescence emission intensity distribution among spots is observed. In Fig. 7C is depicted the accumulated average fluorescence emission intensity distribution across the MB construct immobilized array. The average intensity profile is plotted as pixel intensity (a.u.) as a function of distance (in pixels) in the selected area (yellow lines). The intensity profile is periodic, with sharp peaks with homogeneous distribution and approximately the same intensity. A total of 18 peaks are observed in this average fluorescence emission intensity profile, correlating to each vertical line of the immobilized poly-A MB construct array.

3.4.2 Hybridization of the complementary oligonucleotide sequences to LAMI immobilized MB constructs (poly-A and miRNA-21 specific MB constructs) onto optically flat thiol derivatized quartz surfaces. Immobilization of the miRNA-21 specific MB construct was also carried out and the bioavailability of both poly-A and miRNA-21 MB constructs was tested through visualization of co-localization of the immobilized MB constructs and the respective complementary oligonucleotides by FRET.

The hybridization of immobilized poly-A MB and mi-RNA specific MB constructs with their respective complementary oligonucleotides can be observed in Fig. 8A and 9A. The fluorescence intensity emission of both Cy3 (λ_{em} from ≈570 nm to 650 nm, present in the MBs) and Cy5 (λ_{em} from ≈700 nm to 780 nm, present in the complementary oligonucleotides) was monitored upon excitation at 543 nm (Cy3 excitation wavelength). In Fig. 8A and 9A are depicted Cy3 emission (left) for the immobilized poly-A MB and miRNA-21 MB constructs, respectively, and Cy5 emission (center) for the respective complementary oligonucleotides. Fig. 8A and 9A (right panels) were obtained through an overlap of the respective Cy3 and Cy5 emissions images. Both emissions are spatially overlapped, revealing co-localization of both fluorophores and thus, hybridization between the immobilized MB constructs and their respective complementary oligonucleotides. An average fluorescence emission intensity profile was obtained for each of the individual images as well as a 3D plot of the co-localization images (Fig. 8B and 9B). The confocal fluorescence images obtained for the immobilized poly-A MB array (Cy3 emission, Fig. 8A, left panel) and for the hybridization with the respective complementary poly-T oligonucleotide (Cy5 emission, Fig. 8A, center panel) show a clear profile with sharp and defined peaks (Fig. 8B, left and center panels). The 3D plot of the co-localized Cy3 and Cy5 emissions also shows a defined array pattern, with a homogeneous distribution of the spots inside the array (Fig. 8B, right panel). The array images obtained for the immobilized miRNA-21 specific MB construct (Cy3 emission) and for the hybridized complementary oligonucleotide (Cy5 emission) appear less defined (Fig. 9A, left and center panel, respectively) but the array pattern is still perceptible. The average fluorescence emission intensity profile analysis (Fig. 9B, left and center panel, respectively) reveals the presence of peaks periodically distributed, which location is correlated with each vertical line of the array pattern. These peaks are well defined but less spatially resolved than the peaks observed for the average intensity profile of the images obtained from both the immobilized poly-A MB constructs and the hybridized poly-A MB with its respective complementary oligonucleotide. The 3D plot of the overlapped Cy3 and Cy5 images (immobilized MB construct and complementary oligonucleotide, respectively) shows the co-localization between the immobilized miRNA-21 specific MB and the respective complementary oligonucleotide

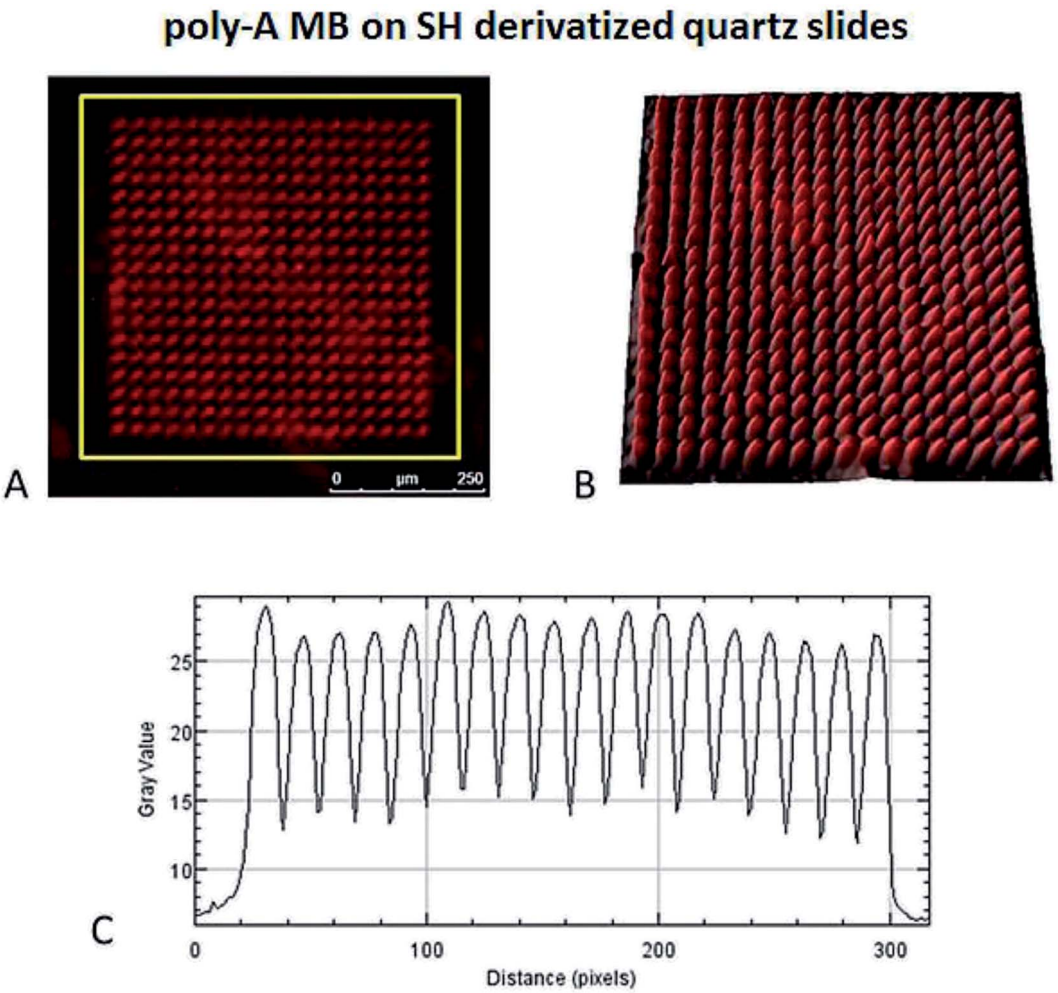

Fig. 7 Analysis of a LAMI immobilized poly-A MB array onto a SH derivatized quartz surface. (A) CFM image of poly-A MB construct immobilized according to an array pattern (20× amplification). (B) 3D surface plot obtained from the analysis of pixel intensity under the selected area in A (yellow box). (C) Correspondent average Cy3 fluorescence emission intensity profile of array in A.

(Fig. 9B, right panel). However, as observed for the individual Cy3 and Cy5 emission images, the spots inside the array pattern are homogenously distributed but poorly resolved, with some background noise between spots.

3.4.3 Control experiments. The same experiments were carried out with the immobilized Cy3 labelled poly-A MB and miRNA-21 specific MB constructs, being the hybridization carried out with the non-complementary Cy5 labelled oligonucleotide strand (poly-A). Cy3 emission is the only observed signal upon excitation of Cy3 (Fig. S5 and S6,† left and right panels). A faint fluorescence signal was detected when exciting Cy3 and specifically opening the detector to detect Cy5 emission (Fig. S5 and S6,† middle panels). This proves that hybridization was not successful and no co-localization between the two fluorophores was visible (Fig. S5 and S6†).

3.4.4 Photonic immobilization of poly-A MB and miRNA-21 specific MB constructs on thiol derivatized SOI surfaces (without PBG sensing structures). The poly-A MB and the miRNA-21 specific MB constructs were placed on a thiol derivatized SOI surface and illuminated at 280 nm according to a line pattern (50 lines, 50 µM separation). In Fig. 10 A1 and B1 are depicted part of the immobilized lines pattern of both MB constructs, observed by CFM. Due to the large size of the arrays, only a portion of each array is visible in the field of view of each image. In Fig. 10A2 and 10B2 are depicted the average fluorescence emission intensity profiles obtained from Fig. 10A1 and 10B1, respectively. Both MB constructs were successfully immobilized onto the thiol derivatized SOI surface. The line pattern of the immobilized poly-A MB construct appears less intense and with thinner lines than the pattern of immobilized miRNA-21 specific MB construct because the light was more focused upon immobilization. The overall fluorescence emission intensity distribution of the immobilized patterns is more homogeneous for the immobilized miRNA-21 specific MB construct (see intensity profile images, Fig. 10A1 and A2). However, for both immobilized MB constructs the peaks appear to be sharp and well defined with a periodic distribution, correlating well with the defined line pattern visualized.

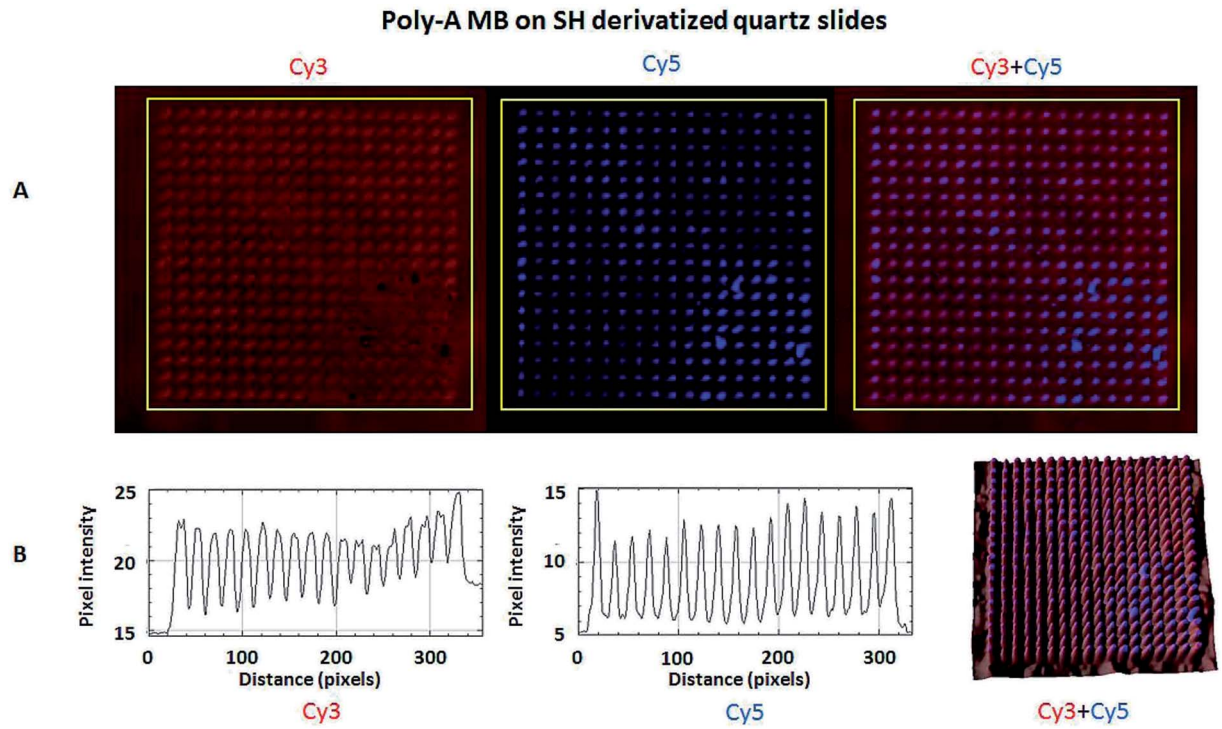

Fig. 8 Bioavailability analysis of a LAMI immobilized poly-A MB arrays onto SH derivatized quartz slides. (A) CFM images of Cy3 labeled poly-A MB constructs fluorescence (left), Cy5 labeled hybridized complementary oligonucleotide fluorescence (centre) and co-localization of Cy3 and Cy5 fluorescence emission (right). (B) Average fluorescence emission intensity profiles of the images in A displayed for Cy3 and Cy5 fluorescence (left and centre) and 3D surface plot of co-localized Cy3 and Cy5 fluorescence emission (right).

3.4.5 Hybridization of the complementary oligonucleotide sequence to LAMI immobilized miRNA-21 specific MB construct onto thiol derivatized SOI surfaces (without PBG sensing structures). The miRNA-21 specific MB construct was illuminated and immobilized onto the SOI surfaces according to a line pattern (see Section 3.4.4.) and hybridized with the target oligonucleotide. The emissions of both the immobilized MB (Cy3 emission) and of the target oligonucleotide (Cy5 emission) were acquired upon excitation at 543 nm (Cy3 excitation) (see Fig. 11A). It is possible to observe the fluorescence of the immobilized MB construct according to a line pattern in the first image (Cy3 emission, left panel) as well as the hybridized complementary oligonucleotide in the second image (Cy5 emission, middle panel). In both images, a defined pattern is observed.

An overlap of both images (Cy3 and Cy5 emissions) was also performed (Fig. 11A, right panel). The co-localization of the immobilized MB construct and the fluorescently labeled oligonucleotide is observed, proving successful hybridization. The 3D plot also shows the overlap, maintaining the resolution of the immobilized pattern and showing that both the immobilization and the hybridization took place in a spatially oriented manner (Fig. 11B).

3.5 Photonic immobilization with LAMI of miRNA-21 specific MB construct photonic-based detection on SOI surfaces with PBG sensing structures – label-free detection

Once the immobilization of the MB probes was tested on SOI surfaces and the detection of their complementary miRNA targets was successfully validated by means of fluorescence-based measurements, a photonic-based detection experiment was performed using nanophotonic sensing structures fabricated on those SOI substrates. To this aim, a photonic chip having several photonic bandgap (PBG) sensing structures (Fig. 4) was used. The photonic sensing chips were biofunctionalised using the LAMI immobilization protocol with diffuse irradiation of the sample instead of focused light. The miRNA-21 specific MB construct was immobilized in two of the PBG sensors pairs while leaving another PBG sensors pair free (*i.e.*, with the organosilane on the surface, but no irradiated miRNA-21 specific MB construct on it). Fig. 12 shows the sensing response for some representative PBG sensing structures on the chip. It can be observed that the PBG sensing structures having the MB construct immobilized are able to detect the presence of the specific target miRNA-21 (red and blue lines), while no sensing response was obtained for that PBG sensor where the MB probe has not been immobilized (green line). The signal obtained for miRNA-21 detection was higher ($\approx 4\times$) for the structure with wider transversal elements ($w_i = 140$ nm, red line) than the signal obtained for miRNA-21 detection from the narrower transversal elements ($w_i = 120$ nm, blue line). Therefore, we can see that the physical parameters of the PBG sensing structure have a dramatic influence on the sensitivity, obtaining a sensing signal ~4 times higher for the structure having wider transversal elements on the PGB sensing structure (red line), what highlights the importance of a proper design in order to obtain an optimized sensitivity.

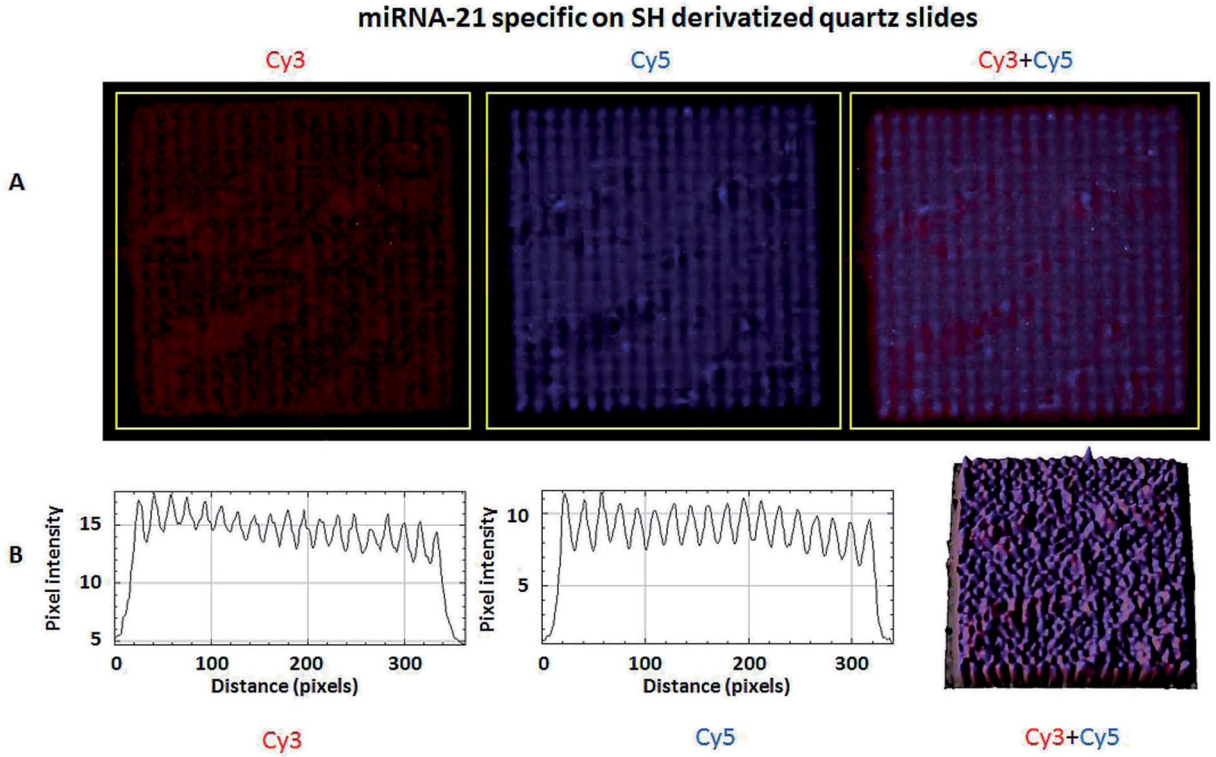

Fig. 9 Bioavailability analysis of a LAMI immobilized miRNA-21 specific MB arrays onto SH derivatized quartz slides. (A) CFM images of Cy3 labeled miRNA-21 MB constructs fluorescence (left), Cy5 labeled hybridized complementary oligonucleotide fluorescence (centre) and co-localization of Cy3 and Cy5 fluorescence images (right). (B) Average fluorescence emission intensity profiles corresponding to the images in C displayed for Cy3 and Cy5 fluorescence (left and centre) and 3D surface plot of co-localized Cy3 and Cy5 fluorescence images (right).

4 Discussion

4.1 Steady state fluorescence studies – hybridization kinetics

The presence of tryptophan in the peptide construct and its proximity to the disulphide bridge is crucial for LAMI. Upon 280 nm excitation, tryptophan undergoes photoionization. The resulting ejected electron is most likely to react with nearby disulphide bridges.[31] A disulphide electron adduct is formed which dissociates, leading to the breakage of the disulphide bridge. As a result, free thiol group(s) will be formed, which covalently bind to thiol derivatized surfaces,[17,30] enabling the spatially oriented immobilization of the MB constructs. The monitored emission spectra upon excitation at 295 nm (wavelength for selective excitation of Trp) displayed a maximum intensity peak at 353 nm. Tryptophan has an emission maximum in water close to 350 nm, being its emission highly dependent on solvent polarity and the surrounding environment.[37] Thus, the presence of this amino acid residue in the peptide was confirmed (see Fig. S4†).

The hybridization rate of poly-A MB (Fig. 6A) and miRNA-21 specific MB (Fig. 6B) constructs with their respective targets is concentration dependent. In general, an initial fast binding phase is observed at all ratios followed by a slower phase until equilibrium is reached. For higher concentrations of oligonucleotide (ratio 1 : 10), this initial phase is almost immediate and equilibrium is reached within minutes (≈2.5 min for poly-A MB and ≈ 6 min for miRNA-21 specific MB). For lower MB/oligonucleotide ratio (1 : 1), this equilibrium is reached at ≈25 min for poly-A MB but for the miRNA MB it can take up to 60 min. Hybridization consists of three steps which, in most cases, happens simultaneously: (a) the target binds to the MB probe domain which remains in a closed loop; (b) the loop opens as the number of bound base pairs increases; (c) binding of target base pairs to the remaining base pairs in the MB.[34] It is reasonable to assume that the hybridization rate is faster in the presence of an excess of oligonucleotide as there is a higher probability for the target sequence to find the MB loop. As concentrations are lowered, steps (a) and (b) are dependent on target sequence/MB loop proximity which might reduce the speed at which these two events occur. Steps (a) and (b) are then the limiting steps for the hybridization reaction and the presence of Cy3 at the stem of the MB does not affect the hybridization rate.[34]

The length of the MB stem also influences the speed at which step (a) occurs. In this study, both poly-A MB and miRNA-21 specific MB have a stem composed of 4 GC base pairs. However, the miRNA-21 specific MB possesses an extra A–T pairing at the stem from the miRNA-21 specific loop. The observed binding kinetics is 17.5× faster for the poly-A MB and its target sequence at a ratio of 1 : 1 (Table 2) when compared with the miRNA-21 MB and its target at a ratio of 1 : 1. This might be due to the simplicity of the sequence as it is composed of a single nucleotide repetition, making it easier for binding to occur. Also, it might be due to the extra A–T pairing in the stem

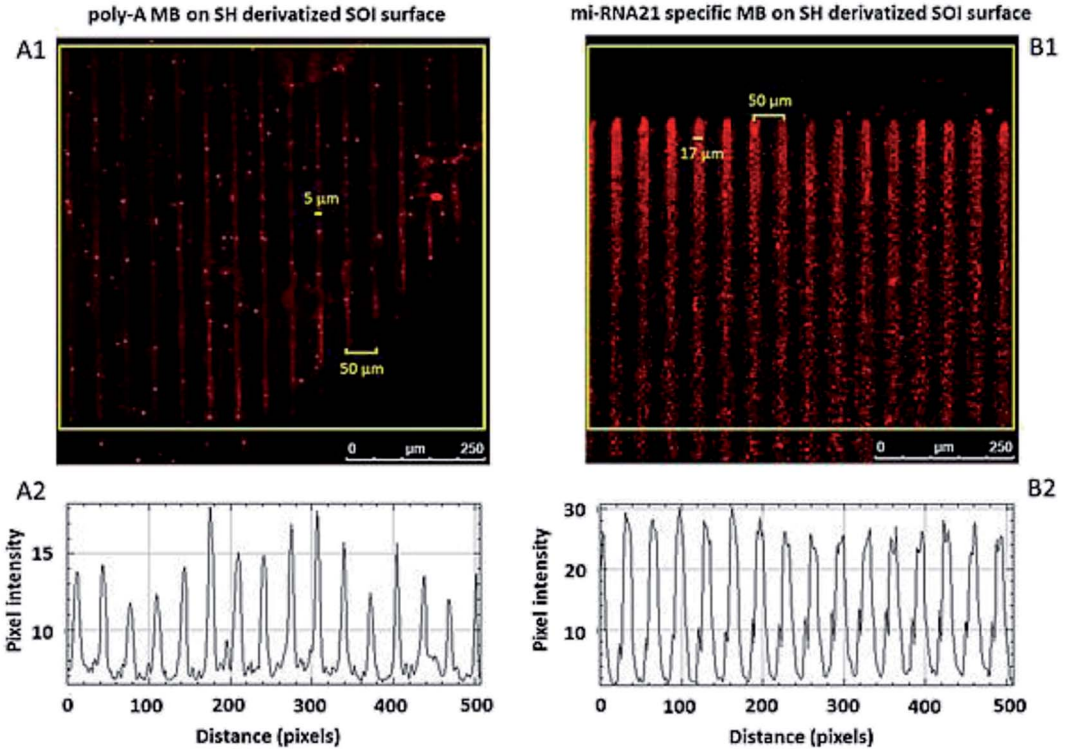

Fig. 10 Analysis of LAMI immobilized poly-A and miRNA-21 MB specific patterns onto SH derivatized SOI surfaces. (A1) CFM image of Cy3 fluorescence emitted by the immobilized poly-A MB construct, according to a line pattern. (A2) Average fluorescence emission intensity corresponding to the immobilized pattern in A1 under the selected area (yellow square). (B1) CFM image of Cy3 fluorescence emitted by the immobilized miRNA-21 specific MB construct, according to a line pattern. (B2) Average fluorescence emission intensity corresponding to the immobilized pattern in B1 under the selected area (yellow square).

of the miRNA-21 specific MB. Nonetheless, the hybridization of the two MBs with their respective complementary oligonucleotide was monitored by two different fluorescence emission processes (unquenching and FRET), which might also influence the observed result.

4.2 Photonic immobilization with LAMI and visual detection of hybridization by CFM

The poly-A MB construct immobilization was successful (Fig. 7) and a spatially oriented immobilization was achieved due to the spatially controlled illumination.

The immobilized poly-A MB construct presents a closed loop conformation, as it has not been exposed to its target sequence. This means that the fluorescence emission of the MB in this state is less intense than when in the open form due to the close spatial proximity of DABCYL (quencher) to Cy3, both present in the stem of the loop (see Fig. 3). However, even in the quenched form, Cy3 fluoresces, allowing the visualization of the immobilized array (see Fig. 7). Such residual Cy3 fluorescence emission was also observed in the initial baseline monitored during the hybridization studies (Fig. 6).

Even though the presence of background fluorescence has been a drawback in the past,[38] data showed that there was a good signal-to-background ratio upon hybridization with the target sequence (S/N ratio below 14.5 for hybridization with miRNA-21 specific and below 3.8 for hybridization with poly-A MB). Furthermore, previous data of immobilized poly-A MB construct showed the increase in the array's fluorescence emission signal upon hybridization with the target sequence due to unquenching.[36] Successful hybridization of the immobilized MB constructs with the target oligonucleotide sequences was also done using FRET (Fig. 8, 9, 10 and 11), both on optically flat thiol derivatized quartz and thiol derivatized SOI surfaces.

The SOI derivatized surfaces are to be integrated in a POC diagnostic device. LAMI presents some advantages over other traditional immobilization techniques. Conventional techniques cannot achieve spatially oriented immobilization of biosensors nor can they assure an immobilized homogeneous monolayer.[39] LAMI is able to achieve covalent immobilization of biosensors in a spatially oriented manner, avoiding the crowding effect that hinders hybridization due to high density of the immobilized probes.[39] Also, LAMI presents high reproducibility and allows for immobilization of proteins, antibodies and MB constructs without compromising the bioavailability of the immobilized biosensors. Furthermore, it does not require high temperatures for hybridization to occur[39] as the hybridization results presented in this paper were obtained at room temperature. Although LAMI uses 280 nm light to achieve immobilization, it does not hinder the biosensors ability to recognize their analytes. UVB light (280–

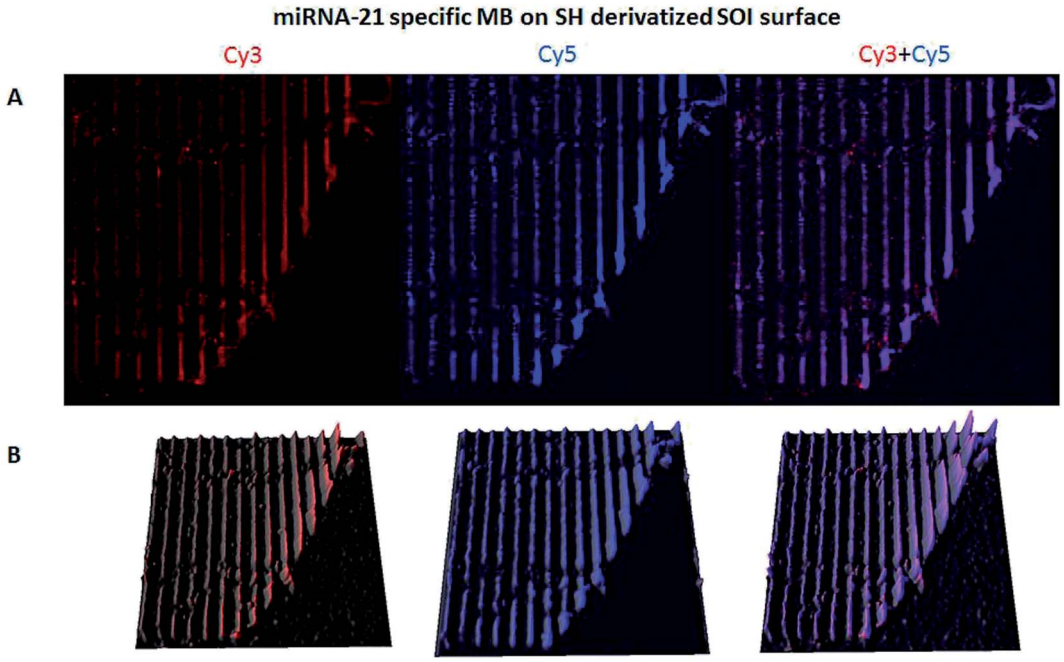

Fig. 11 Bioavailability analysis of LAMI immobilized miRNA-21 specific MB patterns onto SH derivatized SOI surfaces. (A) CFM image of a Cy3 labeled miRNA-21 specific MB construct line array (left), fluorescence emission from the Cy5 labeled and hybridized complementary oligonucleotide fluorescence (centre) and co-localization of Cy3 and Cy5 fluorescence images (right). (B) 3D surface plots of Cy3 labeled miRNA-21 specific MB construct line array (left), Cy5 emission from the hybridized complementary oligonucleotide (centre) and of the co-localized Cy3 and Cy5 emitted fluorescence (right).

315 nm) has been reported to cause damage to DNA. Deamination of bases, depyrimidination and depurination as well as formation of free radicals or reactive oxygen species are some of the UV induced possible changes.[40] However, both immobilized MBs were capable of recognizing the target sequences. Illumination time applied for the immobilization of MB patterns was very short (ms), as the velocity of the moving stage upon illumination was of 100 μm s^{-1}. Thus, the hybridization between the target sequences and the immobilized MB constructs hereby reported was not hindered by the immobilization process.

The excitation wavelength chosen (laser line at 543 nm) for CFM imaging was close to the maximum excitation wavelength described for Cy3 (≈548 nm) and the monitored emission wavelengths correspond to intervals where both Cy3 and Cy5 emit, respectively. At 700 nm (approximate lower limit of the interval in which Cy5 fluorescence emission was monitored), there is almost no fluorescent emission for Cy3 (≈2% relative to its maximum absorption intensity) whereas for Cy5 the fluorescence emission intensity at this wavelength is ≈28%. Furthermore, at the excitation wavelength selected, Cy5 has only a residual absorption of 6% (compared to its maximum absorption intensity).[35] As a consequence, the monitored fluorescence emission intensity is mainly due to FRET, even though some background fluorescence might be visible in the wavelength interval monitored for Cy5 emission. Control experiments where the immobilized Cy3 labelled poly-A MB construct was hybridized with a Cy5 labelled non-complementary oligonucleotides (poly-A oligonucleotide) show that there is no Cy5 emission (upon Cy3 excitation) (Fig. S5†). When using the miRNA-21 MB construct, a faint residual Cy5 signal can be observed (Fig. S6†).

The focal distance also influences the pattern spatial distribution. Fig. 10A1 and B1 show a difference in the thickness of the lines in the immobilized patterns. Although both arrays were designed under the same conditions, a small difference in the focal distance influences the immobilized pattern. The pattern immobilized with more focused light displays lines with ≈5 μm width whereas the pattern immobilized with less focused light displays lines with a width of ≈17 μm, even though both patterns present a distance between lines of 50 μm, as specified in the design. All MB constructs were immobilized with μm resolution.

4.3 Photonic immobilization with LAMI and photonic-based detection on SOI chips with PBG sensing structures – label-free detection

The detection of LAMI immobilized miRNA-21 specific MB using PBG structures was successful. However, it was observed that the sensitivity of detection is dependent on physical parameters such as the width of the transversal elements of the sensing structures and also the presence of SiO_2 in these structures. As the PBG sensing structures need to be in contact with the medium to be analysed, windows are opened in the SiO_2 upper cladding just in the positions where they are placed by UV lithography and etching of the SiO_2. After opening these windows, a more robust photonic chip is obtained, but the presence of some SiO_2 residues in the walls of the PBG sensing structures produces a decrease of its sensitivity. This trade-off

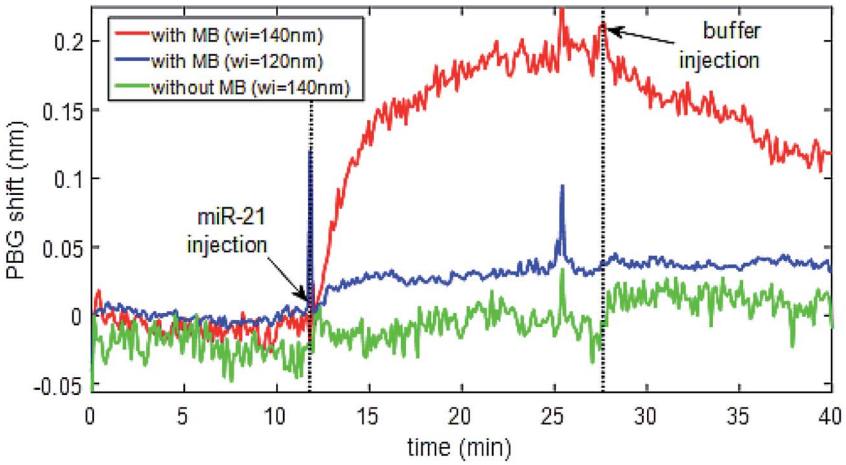

Fig. 12 Spectral evolution of the PBG edge position for the sensing structures within the photonic chip when the target miR-21 is flowed over their surface. The sensing response for PBG sensor is depicted in a different color.

between chip robustness and sensitivity needs to be overcome in future sensing chips developments. The physical parameters of the PBG sensing structure also have a dramatic influence on the sensitivity. The acquired sensing signal for the structure having wider transversal elements of the PGB sensing structure was ~4 times higher (Fig. 12, red line) than the signal obtained for the narrower transversal elements of the PBG sensing structure (Fig. 12, blue line). This sensitivity difference is higher than what it might be expect (around 1.5× from previous experiments), possibly due to the non-uniform presence of the SiO_2 residues from the upper cladding layer. Nanophotonic sensing technology is characterized by a very high sensitivity, which comes from the high interaction occurring between the light confined in the photonic structures and the target analytes in a reduced size structure. Additionally, the type of PBG sensing structures used in this work have demonstrated an even higher sensitivity,[41] which is determined by the appearance of the so-called slow-wave behavior that induces a more effective interaction with the target analyte during a longer time.

5 Conclusions

The new MB constructs presented in this paper were able to recognize target sequences *in vitro*. One of such sequences is a biomarker for colon and breast cancer. The recognition achieved by the two MB constructs was assessed by two different fluorescence recognition methods. These constructs were successfully immobilized onto thiol reactive surfaces using LAMI. LAMI presents some advantages over more conventional immobilization techniques as it allows for immobilization in spatially oriented and covalent manner and with μm resolution (sub-μm resolution can also be achieved).[22,23] Biosensors bioavailability is not compromised by the UV light used for immobilization, making these biosensors and LAMI suitable to produce arrays for integration in POC diagnostic devices and used in this specific project for the detection of cancer biomarkers.

Conflicts of interest

The authors declare no conflicts of interest.

Acknowledgements

This work was supported by the European Commission through the project H2020-644242 – SAPHELY and the project H2020-634013-2-PHOCNOSIS.

References

1 New Global Cancer Data: GLOBOCAN 2018|UICC, https://www.uicc.org/new-global-cancer-data-globocan-2018, accessed 14 December 2018.
2 WHO|Cancer, http://www.who.int/cancer/en/, accessed 14 December 2018.
3 WHO|Cancer, http://www.who.int/mediacentre/factsheets/fs297/en/, accessed 16 August 2017.
4 Y. Li, C. Qiu, J. Tu, B. Geng, J. Yang, T. Jiang and Q. Cui, *HMDD v2.0: a database for experimentally supported human microRNA and disease associations*, https://academic.oup.com/nar/article-lookup/doi/10.1093/nar/gkt1023, accessed 16 August 2017.
5 G. A. Calin, C. D. Dumitru, M. Shimizu, R. Bichi, S. Zupo, E. Noch, H. Aldler, S. Rattan, M. Keating, K. Rai, L. Rassenti, T. Kipps, M. Negrini, F. Bullrich and C. M. Croce, *Proc. Natl. Acad. Sci. U. S. A.*, 2002, **99**, 15524–15529.
6 M. D. Jansson and A. H. Lund, *Mol. Oncol.*, 2012, **6**, 590–610.
7 Y. S. Lee and A. Dutta, *Annu. Rev. Pathol.*, 2009, **4**, 199–227.
8 S. Volinia, G. A. Calin, C.-G. Liu, S. Ambs, A. Cimmino, F. Petrocca, R. Visone, M. Iorio, C. Roldo, M. Ferracin, R. L. Prueitt, N. Yanaihara, G. Lanza, A. Scarpa, A. Vecchione, M. Negrini, C. C. Harris and C. M. Croce, *Proc. Natl. Acad. Sci. U. S. A.*, 2006, **103**, 2257–2261.
9 J. Iqbal, Y. Shen, X. Huang, Y. Liu, L. Wake, C. Liu, K. Deffenbacher, C. M. Lachel, C. Wang, J. Rohr, S. Guo,

L. M. Smith, G. Wright, S. Bhagavathi, K. Dybkaer, K. Fu, T. C. Greiner, J. M. Vose, E. Jaffe, L. Rimsza, A. Rosenwald, G. Ott, J. Delabie, E. Campo, R. M. Braziel, J. R. Cook, R. R. Tubbs, J. O. Armitage, D. D. Weisenburger, L. M. Staudt, R. D. Gascoyne, T. W. McKeithan and W. C. Chan, *Blood*, 2015, **125**, 1137–1145.

10 S. Thakur, R. K. Grover, S. Gupta, A. K. Yadav and B. C. Das, *PLoS One*, 2016, **11**, e0158946.

11 A. Bunschoten, T. Buckle, J. Kuil, G. D. Luker, K. E. Luker, O. E. Nieweg and F. W. B. van Leeuwen, *Biomaterials*, 2012, **33**, 867–875.

12 C. Glinge, S. Clauss, K. Boddum, R. Jabbari, J. Jabbari, B. Risgaard, P. Tomsits, B. Hildebrand, S. Kää, R. Wakili, T. Jespersen and J. Tfelt-Hansen, *PLoS One*, 2017, **12**(2), e0167969.

13 P. S. Mitchell, R. K. Parkin, E. M. Kroh, B. R. Fritz, S. K. Wyman, E. L. Pogosova-Agadjanyan, A. Peterson, J. Noteboom, K. C. O'Briant, A. Allen, D. W. Lin, N. Urban, C. W. Drescher, B. S. Knudsen, D. L. Stirewalt, R. Gentleman, R. L. Vessella, P. S. Nelson, D. B. Martin and M. Tewari, *Proc. Natl. Acad. Sci. U. S. A.*, 2008, **105**, 10513–10518.

14 J. A. Weber, D. H. Baxter, S. Zhang, D. Y. Huang, K. H. Huang, M. J. Lee, D. J. Galas and K. Wang, *Clin. Chem.*, 2010, **56**(11), 1733–1741.

15 Globocan 2012 – Home, http://globocan.iarc.fr/Default.aspx, accessed 16 August 2017.

16 M. T. Neves-Petersen, T. Snabe, S. Klitgaard, M. Duroux and S. B. Petersen, *Protein Sci.*, 2006, **15**, 343–351.

17 M. T. Neves-Petersen, M. Duroux, E. Skovsen, L. Duroux and S. B. Petersen, *J. Nanosci. Nanotechnol.*, 2009, **9**, 3372–3381.

18 E. Skovsen, T. Neves-Petersen, L. Duroux and S. Petersen, Advanced Biomedical and Clinical Diagnostic Systems VI, *Proc. of SPIE*, 2008, vol. 6848, p. 68480O-1.

19 E. Skovsen, M. Duroux, M. T. Neves-Petersen, L. Duroux and S. B. Petersen, *Int. J. Optomechatronics*, 2007, **1**, 383–391.

20 M. Duroux, E. Skovsen, M. T. Neves-Petersen, L. Duroux, L. Gurevich and S. B. Petersen, *Proteomics*, 2007, **7**, 3491–3499.

21 E. Skovsen, M. T. Neves-Petersen, A. Kold, L. Duroux and S. B. Petersen, *J. Nanosci. Nanotechnol.*, 2009, **9**, 4333–4337.

22 E. Skovsen, A. B. Kold, M. T. Neves-Petersen and S. B. Petersen, *Proteomics*, 2009, **9**, 3945–3948.

23 S. B. Petersen, A. Kold di Gennaro, M. T. Neves-Petersen, E. Skovsen and A. Parracino, *Appl. Opt.*, 2010, **49**, 5344–5350.

24 P. Jonkheijm, D. Weinrich, H. Schröder, C. M. Niemeyer and H. Waldmann, *Angew. Chem., Int. Ed.*, 2008, **47**, 9618–9647.

25 D. S. Wilson and S. Nock, *Curr. Opin. Chem. Biol.*, 2002, **6**, 81–85.

26 B. Johnsson, *Anal. Biochem.*, 1991, **277**, 268–277.

27 A. Collioud, J. F. Clémence, M. Sänger and H. Sigrist, *Bioconjugate Chem.*, 1993, **4**, 528–536.

28 R. Y. Sweeney, B. R. Kelemen, K. J. Woycechowsky and R. T. Raines, *Anal. Biochem.*, 2000, **286**, 312–314.

29 M. T. Petersen, P. H. Jonson and S. B. Petersen, *Protein Eng.*, 1999, **12**, 535–548.

30 M. T. Neves-Petersen, Z. Gryczynski, J. Lakowicz, P. Fojan, S. Pedersen, E. Petersen and S. B. Petersen, *Protein Sci.*, 2002, **11**, 588–600.

31 M. T. Neves-Petersen, S. Klitgaard, T. Pascher, E. Skovsen, T. Polivka, A. Yartsev, V. Sundström and S. B. Petersen, *Biophys. J.*, 2009, **97**, 211–226.

32 *Black Hole Quencher® Dyes|LGC Bioresearch Technologies*, https://www.biosearchtech.com/support/education/fluorophores-and-quenchers/black-hole-quencher-dyes, accessed 12 December 2017.

33 M. Zuker, *Nucleic Acids Res.*, 2003, **31**, 3406–3415.

34 A. Tsourkas, M. A. Behlke, S. D. Rose and G. Bao, *Nucleic Acids Res.*, 2003, **31**, 1319–1330.

35 Thermo Fisher Scientific Inc., Fluorescence SpectraViewer, https://www.thermofisher.com/dk/en/home/life-science/cell-analysis/labeling-chemistry/fluorescence-spectraviewer.html, accessed 7 November 2017.

36 O. Gonçalves, S. Snider, R. Zadoyan, Q.-T. Nguyen, H. Vorum, S. B. Petersen and M. T. Neves-Petersen, Reporters, Markers, Dyes, Nanoparticles, and Molecular Probes for Biomedical Applications IX, *Proc. of SPIE*, 2017, vol. 10079, p. 100790F-1.

37 J. R. Lakowicz, *Principles of fluorescence spectroscopy*, Academic/Plenum Publishers, New York, 2nd edn, 1999.

38 C. S. Wu, L. Peng, M. You, D. Han, T. Chen, K. R. Williams, C. J. Yang and W. Tan, *Int. J. Mol. Imaging*, 2012, **2012**, 501579.

39 S. B. Nimse, K. Song, M. D. Sonawane, D. R. Sayyed and T. Kim, *Sensors*, 2014, **14**, 22208–22229.

40 R. P. Rastogi, A. K. Richa, M. B. Tyagi and R. P. Sinha, *J. Nucleic Acids*, 2010, **2010**, 592980.

41 Á. Ruiz-Tórtola, F. Prats-Quílez, D. González-Lucas, M.-J. Bañuls, Á. Maquieira, G. Wheeler, T. Dalmay, A. Griol, J. Hurtado and J. García-Rupérez, *Biomed. Opt. Express*, 2018, **9**, 1717–1727.